frontiers | Frontiers in Materials

TYPE Original Research
PUBLISHED 10 January 2023
DOI 10.3389/fmats.2022.1088554

OPEN ACCESS

EDITED BY
Zhigang Zhang,
Chongqing University, China

REVIEWED BY
M. Iqbal Khan,
King Saud University, Saudi Arabia
Yang Zou,
Chongqing Jiaotong University, China

*CORRESPONDENCE
A. Deifalla,
ahmed.deifalla@fue.edu.eg,
diffalaf@mcmaster.ca
Mahmood Ahmad,
ahmadm@uetpeshawar.edu.pk

SPECIALTY SECTION
This article was submitted to Structural Materials, a section of the journal Frontiers in Materials

RECEIVED 03 November 2022
ACCEPTED 21 December 2022
PUBLISHED 10 January 2023

CITATION
Awad A, Tawfik M, Deifalla A, Ahmad M, Sabri Sabri MM and El-said A (2023), Effect of hybrid-fiber- reinforcement on the shear behavior of high-strength-concrete beams.
Front. Mater. 9:1088554.
doi: 10.3389/fmats.2022.1088554

Effect of hybrid-fiber-reinforcement on the shear behavior of high-strength-concrete beams

Ahmed Awad[1], Maged Tawfik[2], A. Deifalla[3]*, Mahmood Ahmad[4]*, Mohanad Muayad Sabri Sabri[5] and Amr El-said[2]

[1]Faculty of Engineering, October University for Modern Sciences and Arts, Giza, Egypt, [2]Department of Civil Engineering, The Higher Institute of Engineering, El Shrouk, Cairo, Egypt, [3]Structural Engineering and Construction Management Department, Future University in Engineering, Cairo, Egypt, [4]Department of Civil Engineering, University of Engineering and Technology Peshawar (Bannu Campus), Bannu, Pakistan, [5]Peter the Great St. Petersburg Polytechnic University, St. Petersburg, Russia

The shear behavior of concrete beams is highly affected by the implementation of better performance concrete. Hybrid fibers addition to concrete mixture has proven to improve the performance compared to just using single type of fiber. Thus, in this current study, the shear behavior of hybrid-fiber-reinforced-high-strength-concrete beams was investigated experimentally. In addition, the effect of the span-to-depth ratio and the transverse reinforcement ratio were examined. Results showed that, when .45% of the cement weight is replaced with polypropylene fiber and 7% of the cement weight is replaced with steel fibers, the shear strength of the beam was enhanced by 18% in comparison to the control beam. The Formation and progression of cracks were also better controlled. The behavior of hybrid-polypropylene-steel-fibers-high-strength-concrete beams was observed to be comparable to that of conventional concrete ones as the shear strength increased with the decrease in span to depth ratio or the increase in transverse reinforcing ratio. A non-linear numerical model was developed and validated using the experimental results. The shear capacities of beams were calculated using ACI, which was compared to experimental and numerical results. The ACI's calculations were conservative when compared with the experimental or numerical results. The coefficient of variance between the ACI and experimental shear capacity results was 4.8%, while it was 9.2% between the ACI and numerical shear capacity results.

KEYWORDS

shear, fiber, steel, polyproplene, beams

1 Introduction

The reinforced concrete (RC) evolution have been an ongoing process with so many advancements (Ahmad et al., 2022; Ahmed et al., 2022; Ali et al., 2022; Ashraf et al., 2022; Ghareeb et al., 2022; Huang et al., 2022; Khan et al., 2022; Li et al., 2022; Mohammed et al., 2022; Shen et al., 2022; Zou et al., 2023a; Zou et al., 2023b). High-strength concrete (HSC), especially that with fiber-RC (FRC) is a versatile form of a concrete mixture with superior performance compared to that of normal RC without fiber reinforcement (Deifalla, 2021a; Deifalla et al., 2021). Higher cement demand during the production of HSC resulted in the consumption of resources and environmental issues (Juenger et al., 2019; Naqi and Jang, 2019). Researchers turned to add single or hybrid fibers to the concrete mixture as an alternative to cement to limit environmental destruction. Additionally for the significance of these fibers in enhancing

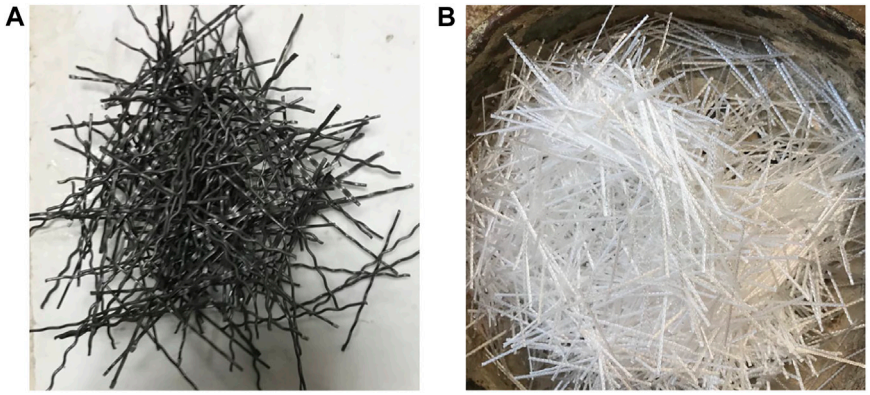

FIGURE 1
Shape of **(A)** steel fiber and **(B)** polypropylene fiber.

TABLE 1 Properties of steel fibers and polypropylene fibers.

Fiber type	Length (mm)	Cross-section	Modulus of elasticity (GPa)	Tensile strength (MPa)
Steel	35	1 mm × 4 mm	211	2,550
Polypropylene	20	Diameter of .04 mm	69	2,075

concrete's behavior in resisting tensile stresses and minimizing the formation and propagation of cracks. The findings of earlier studies demonstrated that utilizing hybrid fibers enhanced concrete strength and durability as well as minimized cracks compared to using a single type of fiber (Hoang and Fehling, 2017; Li et al., 2018; Zhang et al., 2018; Ali et al., 2020; Sivakumar et al., 2020; Zhong et al., 2020; Tawfik et al., 2022). Tawfik et al. (2022) observed that using hybrid fibers rather than only one kind of fiber increased the strength of the composite in terms of compressive, flexural, and tensile stresses by 50%, 46%, and 53%, respectively. This improvement in strength is caused by the incorporation of hybrid fibers with various characteristics, which stop the development of multiscale crack formation at various levels of stress. When incorporated into cementitious materials, fibers with such a greater young's modulus enhance the compressive behavior of concrete by suppressing the growth of macro-cracks at high-stress levels. Additionally, fibers with a minimal young's modulus massively increase concrete compressive behavior by restricting the forming of micro-cracks at small levels of stress.

Prior studies proved that the shear behavior of RC beams significantly enriched due to the steel fibers inclusion. Yavaş et al. (2019) concluded that the use of different volume content (1.5%, 1%, and .5%) of steel fibers, various lengths (6 mm, 13 mm, 30 mm, and 60 mm) of steel fibers, and several shapes (straight, double hooked, and hooked) of steel fibers. These additions enhanced the shear strength of ultrahigh strength FRC (UHSFRC) beams more than the control beam. Furthermore, using 1.5% straight steel fiber as a partial substitute for cement and with a length of 13 mm had the best impact on shear strength and cracking pattern for UHSFRC beams. Similar findings were produced by Lim and Hong (2017), who found that adding steel fiber with a volume content of 1.5% into UHSFRC beams resulted in a significant increase in shear strength. Shear reinforcement additionally improved the ductility of concrete beams. According to earlier research, steel fibers can be used instead of the transverse reinforcement in concrete beams while sustaining ductility and shear strength, or even perform a little bit better. Tahenni et al. (2016) explored that high-strength concrete beams without transverse reinforcing and having steel fibers with volume content up to 3% displayed slightly better shear behavior than high-strength concrete beams with transverse reinforcing and without steel fibers. The FRC beams showed improved shear strength and relatively minimal diagonal cracks, especially for steel fiber volume content from 1% to 3%. Also, Torres and Lantsoght (2019) revealed that the minimum transverse reinforcement required by ACI318 can be replaced by steel fibers in the amount of 1.2%, whereas the minimum transverse reinforcement required by Eurocode two can be replaced by steel fibers in the amount of .6%.

Even though the use of polypropylene fibers in concrete did not provide that resistance to shear stresses as steel fibers, it was demonstrated that it would be possible to slightly improve the behavior of the concrete beams in terms of cracking load, crack bridging, and shear capacity. Yang et al. (2021) showed that the inclusion of polypropylene fiber could further enhance the shear strength of concrete beams by up to 17% when compared to reinforced-concrete beams without fibers. Additionally, the presence of polypropylene fiber improved the initial crack shear load, prevented crack progression, maximized the number of cracks, and decreased crack width, thereby helping to increase beam ductility and improve strength properties. Ortiz Navas et al. (2018) demonstrated that the shear strength of FRC beams with or without stirrups increased noticeably when 10 kg/m^3 of polypropylene fibers were added, compared to the control specimens. The failure modes of fiber concrete beams with stirrups and those without stirrups were comparable.

TABLE 2 Mix properties.

Mix	Polypropylene fiber volume (%)	Steel fiber volume (%)	Silica fume (Kg/m3)	Cement (Kg/m3)	W/C ratio	Coarse Agg. (Kg/m3)	Fine Agg. (Kg/m3)	Super plasticizer (Lit./m3)
Control Mix	—	—	25	500	.40	1148	705	6.4
Hybrid fibers Mix	.45	7	25	463	.40	1148	705	6.4

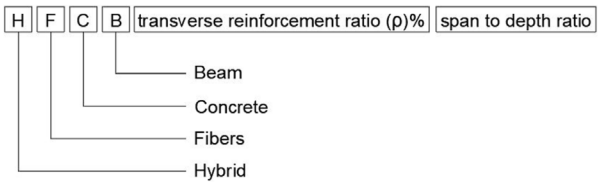

FIGURE 2
Designation for all concrete beams.

Few studies have focused on the impact of applying hybrid fibers rather than a single type on the shear behavior of concrete beams since, as was earlier mentioned, hybrid fibers provide improved mechanical properties and can control cracks at various stress levels. Shaaban et al. (2021) evaluated the effect of various shapes of silica fume, polyvinyl alcohol, polypropylene, or hybrid fibers on the shear behavior of reinforced concrete beams experimentally and numerically. When comparing the control beam which contains transverse reinforcement and no fibers, introducing hybrid fibers, increased shear strength and ductility. Hybrid fibers with .75% polyvinyl alcohol and .75% polypropylene and transverse reinforcement produced greater shear capacity and ductility when compared to beams without transverse reinforcement and containing hybrid fibers with 1.5% polyvinyl alcohol and .375% polypropylene. Depending upon these findings, it was suggested that hybrid fibers with .75% polyvinyl alcohol and .75% polypropylene, as well as stirrup reinforcement (7.5 Ø 6/m), be employed to accomplish high shear strength for hybrid FRC beams. The finite element predictions for the tested beams exhibited a strong agreement with the experimental observations regarding the shear capacity, maximum deflection, and failure pattern. Ismail and Hassan. (2021) explored the shear performance of FRC using various fiber kinds. Polyvinyl alcohol fiber lengths of 8 and 12 mm, polypropylene fibers length of 19 mm, and steel fibers length of 13 mm were the four different kinds of fiber employed. According to the findings, all FRC beams outperformed the control beam on basis of cracking behavior, shear strength, ductility, and energy absorption. The FRC beam containing polyvinyl alcohol fibers with 8 mm length showed higher shear strength and ductility than the FRC beam containing polyvinyl alcohol fibers with 12 mm length. Polypropylene FRC beams performed the least, whereas steel FRC beams performed the best in terms of first crack load, maximum strength, ductility, and ability to absorb energy. According to Alrefaei et al. (2018), inserting hybrid polypropylene-steel fibers up to a volume of 2% was significant in improving the shear capacity by approximately eight times compared to the concrete beams without fibers. Furthermore, the beams' ductility, multi-cracking behavior, and concrete strain capability were all significantly enhanced. It is demonstrated that, regardless of the hybridized ratio, a hybrid fiber volume content of 1% is a sufficient minimum transverse reinforcement for concrete beams having compression strength varying between 40 and 65 MPa.

The majority of previous work focused on the physical and mechanical characteristics of using single or hybrid fibers in cementitious materials (Tahenni et al., 2016; Lim and Hong, 2017; Alrefaei et al., 2018; Ortiz Navas et al., 2018; Zhang et al., 2018; Ayub et al., 2019; Koniki and Prasad, 2019; Torres and Lantsoght, 2019; Xu et al., 2019; Yavaş et al., 2019; Ali et al., 2020; Ismail and Hassan, 2021; Shaaban et al., 2021; Yang et al., 2021), and there have been fewer studies on the shear behavior of FRC elements that used a single type of fiber, whereas there is a lack of research into the effect of hybrid fibers on the shear behavior of high-strength concrete elements although the use of hybrid fibers had been shown to significantly improve the properties of concrete over the use of a single type of fiber (Alrefaei et al., 2018; Navas et al., 2018; Khan et al., 2020). Additionally, the previous studies that used hybrid fibers varied in terms of the type, proportion, characteristics, and shape of the fibers (Kumar et al., 2017; Fadil et al., 2018; Smarzewski, 2018; Wang et al., 2019; Zhang et al., 2019; Shi et al., 2020; Tran et al., 2020). As a result, prospective studies in this area are required to produce meaningful results. From this viewpoint, the current research was conducted to study experimentally and numerically the shear behavior of HFRHSC beams. The main parameters were concrete type, span to depth ratio, and transverse reinforcement ratio.

2 Experimental program

2.1 Materials and mix proportions

HSC was produced using cement, pure water, fine aggregate, coarse aggregate, silica fume, superplasticizer, and hybrid polypropylene-steel fibers. The cement used was ordinary Portland cement. The coarse aggregate was formed of crushed dolomite with a particle size of 10 mm and an apparent specific gravity of 2.6, while the fine aggregate was a siliceous natural with a fineness modulus of 3.35. Silica fume was added to the concrete mixture to fill the voids and thus improve the strength, while a superplasticizer was added to improve the workability of the concrete. The forms of the fibers are shown in Figure 1 and Table 1 displays the steel and polyethylene fiber characteristics as reported by the suppliers. The binder component was dry-mixed for about 3 min in a mechanical mixer before adding the full quantity of water and superplasticizer to the concrete mixture. Polypropylene and steel fibers were added to the mixture after the wet mixing process and mixed for around 5 min. The transverse reinforcement showed a tensile yield strength of 240 MPa and

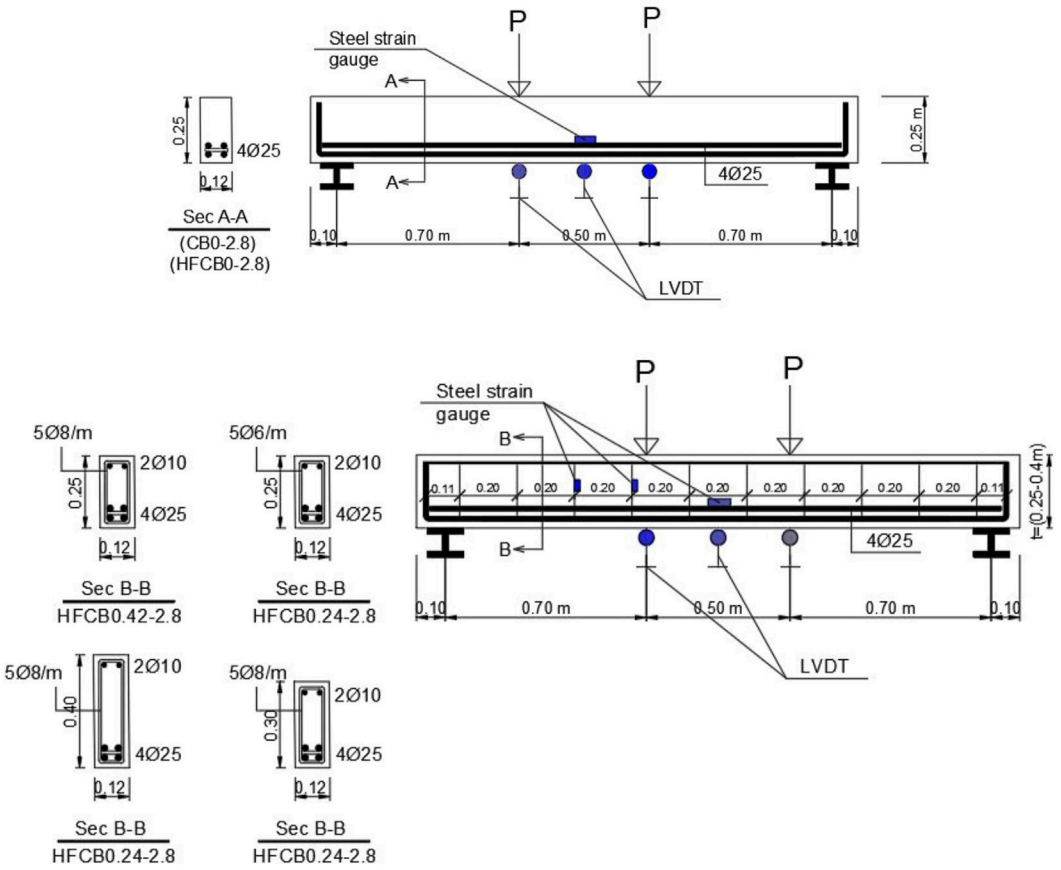

FIGURE 3
Typical dimensions, reinforcement, and instruments for all concrete beams.

TABLE 3 Details of all concrete beams.

Beam ID	Concrete type	Cross section cm^2	Stirrups	Transverse reinforcement ratio (ρ) %	Longitudinal reinforcement	Shear span cm	Span-to-depth ratio
CB0-2.8	Normal	12 × 25	—	0	4Ø25 Bottom 2Ø10 Upper	70	2.8
HFCB0-2.8	Hybrid	12 × 25	—	0		70	2.8
HFCB0.24-2.8	Hybrid	12 × 25	5Ø6/m	.24		70	2.8
HFCB0.42-2.8	Hybrid	12 × 25	5Ø8/m	.42		70	2.8
HFCB0.42-2.3	Hybrid	12 × 30	5Ø8/m	.42		70	2.8
HFCB0.42-1.75	Hybrid	12 × 40	5Ø8/m	.42		70	2.8

ultimate strength of 385 MPa, compared to the longitudinal reinforcement's tensile yield strength of 520 MPa and ultimate strength of 690 MPa. The mix quantities, which are based on Tawfik et al. (2022) are shown in Table 2. For the best mechanical characteristics in terms of compressive, tensile, flexural strength, and cracking control, the concrete mixture contains .45% of polypropylene fiber and 7% of steel fiber as a replacement ratio for the cement weight.

2.2 Description and preparation of beam specimens

Five hybrid-polypropylene-steel-fiber-reinforced-high-strength-concrete (HFRHSC) beams and one control high-strength reinforced concrete beam are included in the experimental program. The beams are labeled according to the shown in Figure 2. The control beam (CB0-2.8) was 120 mm and 250 mm in

FIGURE 4
Preparation of concrete beams.

FIGURE 5
Test setup for all concrete beams.

width and depth, respectively, while being 2,100 mm long, with no stirrups or fibers, and the flexure longitudinal reinforcement used was 4Ø25. All HFRHSC beams contain 7.45% hybrid fibers as a substitute for the weight of cement, which was divided into 7% steel fibers and .45% polypropylene fibers. The first hybrid FRC beam (HFCB0-2.8), was similar to the control beam in dimensions and proportion of longitudinal steel reinforcement, but the difference was the presence of a hybrid of polypropylene-steel fibers. The second hybrid FRC beam (HFCB0.24-2.8), was similar to the concrete beam (HFCB0-2.8) in dimensions, concrete type, and proportion of longitudinal steel reinforcement, except for the presence of 5Ø6/m transverse reinforcement. The transverse reinforcement ratio of the hybrid FRC beam (HFCB0.42-2.8) was higher than that of the concrete beam (HFCB0.24-2.8), while the dimensions, concrete type, and longitudinal reinforcement ratio were the same in both concrete beams. The hybrid FRC beams (HFCB0.42-2.3) and (HFCB0.42-1.75) differed from the concrete beam (HFCB0.42-2.8) in depth, which was 300 mm and 400 mm, respectively, however, they were similar in terms of width, length, concrete type, and proportion of longitudinal and transverse steel reinforcement. Figure 3 and Table 3 show the details for all concrete beams. To evaluate the mechanical characteristics, including compressive strength, tensile strength, and modulus of elasticity, six concrete cubes (150 × 150 × 150 mm) and 12 concrete cylinders (150 × 300 mm for diameter and height, respectively) were taken from that concrete mixture of each beam. The samples were prepared and examined as per the Egyptian code of concrete specifications.

The transverse reinforcement ratio (ρ) can be calculated using Eq. 1 as the area of transverse reinforcement (Av) multiplied by the spacing between stirrups (s) and the width of the beam (b).

$$\rho = \frac{Av}{b \times s}\% \quad (1)$$

The wooden forms of all concrete beams were prepared and thoroughly sprayed with water before the pouring process to maintain the water in the mixture and not being absorbed by the wood. Electrical strain gauges with a length of 10 mm and a resistance of 120.3 ± .5 Ω were attached to the longitudinal and transverse reinforcement bars in the location as seen in Figure 3, which is responsible for monitoring the strain in the reinforcements along the loading history. The reinforcement was then positioned in the forms as illustrated in Figure 4. The casting process then began, with a vibrator used during the casting to prevent separation between the concrete mortar and the coarse aggregate and to ensure regular fibers distribution. Following 24 h of casting, the forms were withdrawn, and the concrete beams were continually moistened with water for 28 days before being examined.

2.3 Test setup of beam specimens

Figure 5 illustrates the testing procedure used to examine the shear behavior of HFRHSC beams. The beams were supported by two

TABLE 4 Density, flexural, compressive strength, and modulus of elasticity results for control and hybrid FRC specimens.

Mix	Density (kg/m^3) at	Strength compressive (MPa)		Strength flexural (MPa)		Young's modulus (GPa)	
	28 days	7 days	28 days	7 days	28 days	7 days	28 days
Control mix	3,362 ± 90	30.2 ± 1.2	48 ± 1.8	3.2 ± 0.2	4.9 ± 0.2	21.5 ± 0.9	31 ± 1.2
Hybrid fibers mix	3,365 ± 75	49 ± 1	75 ± 1.5	4.1 ± 0.1	5.5 ± 0.3	28 ± 1	38 ± 1.4

TABLE 5 Experimental results for all concrete beams.

Beam ID	Shear load V (kN)		Mid-span deflection Δ (mm)		Strain at stirrups ε %		Strain at long. Reinforcement ε %		[a]Ductility ratio
	$V_{Failure}$	$V_{Cracking}$	$\Delta_{Failure}$	$\Delta_{Cracking}$	$\varepsilon_{Failure}$	$\varepsilon_{Cracking}$	$\varepsilon_{Failure}$	$\varepsilon_{Cracking}$	
CB0-2.8	45	12	2.84	1.56	—	—	.06	.017	1.82
HFCB0-2.8	53	20	3.19	1.10	—	—	.07	.018	2.90
HFCB0.24-2.8	71	31	3.89	1.21	.13	2.67E-03	.09	.034	3.21
HFCB0.42-2.8	80	37	4.11	1.09	.14	1.23E-03	.10	.045	3.76
HFCB0.42-2.3	111	52	4.80	1.80	.13	1.98E-03	.10	.047	2.66
HFCB0.42-1.75	137	60	4.04	1.74	.16	1.68E-03	.11	.054	2.32

[a]Ductility ratio = ($\Delta_{Failure}/\Delta_{Cracking}$).

supports (hinged and roller), with a distance of 2,000 mm between them. The load was applied using a hydraulic jack positioned in the middle of the beam. The hydraulic jack's load was transmitted through an I-steel beam so that it concentrated symmetrically in two points, provided that the distance between the concentrated load and the support was 700 mm on either side. Three LVDTs were installed in the critical sections as shown in Figure 5 to monitor the displacement values during loading. The deflection of concrete beams and reinforcement strain were measured every 10 kN of loading, as well as cracks, were marked. The load steadily increased until the concrete beam collapsed.

3 Results

3.1 Mechanical properties

Table 4 displays the mechanical properties of the concrete mix implemented for the casting of the specimens, which are represented in tensile and compressive strength as well as modulus of elasticity. The results were calculated as the average of three samples tested under the same conditions. For each mix, six cube specimens with a cross-section of 15 cm × 15 cm, and a height of 15 cm were implemented to measure the compressive strength. Three cube specimens were tested at 7-day, and three as well at 28-day. Furthermore, the elastic modulus was determined for each cementitious material by examining concrete cylinder specimens at 7-day as well as another three at 28-day. The cylinder specimens have a diameter of 15 cm and a height of 30 cm. Whereas the flexural strength of each cementitious material is evaluated by examining three concrete beam specimens at 7-day as well as three more at 28-day. The concrete beams have all been 70 cm long, 15 cm × 15 cm in cross-section.

3.2 Shear behavior of concrete beam specimens

This section displays the results of (shear load, mid-span deflection, and ductility) at the failure and cracking stages for every concrete beam specimen. Furthermore, relationships between load and various parameters such as mid-span deflection, stirrup strain, and longitudinal bar strain were studied. The strain in the stirrup was calculated by taking the average of the two strain gauges installed in the stirrup's vertical legs in the critical shear zone. While the longitudinal reinforcement strain was measured at the maximum flexure stress, which is at mid-span. Table 5 represents the experimental results for all concrete beams.

3.2.1 Load versus deflection for all concrete beams

The relationship between load and mid-span deflection for all concrete beams is illustrated in Figure 6. According to the findings, the mid-span deformation values at the first shear crack for concrete beams CB0-2.8, HFCB0-2.8, HFCB0.24-2.8, HFCB0.42-2.8, HFCB0.42-2.3, and HFCB0.42-1.75 were 1.56, 1.1, 1.21, 1.09, 1.8, and 1.74 mm, respectively. Additionally, the concrete beams CB0-2.8, HFCB0-2.8, HFCB0.24-2.8, HFCB0.42-2.8, HFCB0.42-2.3, and HFCB0.42-1.75 had maximum mid-span deformation values of 2.84, 3.19, 3.89, 4.11, 4.8, and 4.04 mm, respectively. It was noticeable that hybrid FRC beams with or without transverse steel reinforcement showed lower deformation values than the control beams CB0-2.8 at the same load, demonstrating the ability of fibers

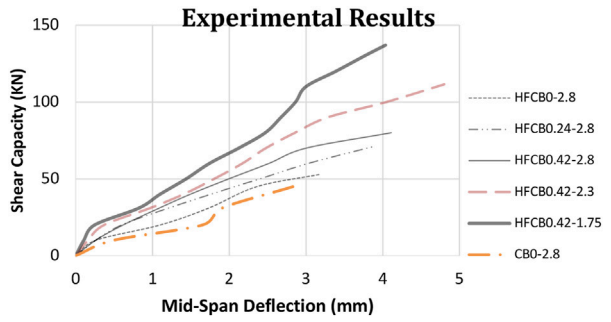

FIGURE 6
The relation between load and mid-span deflection for all concrete beams.

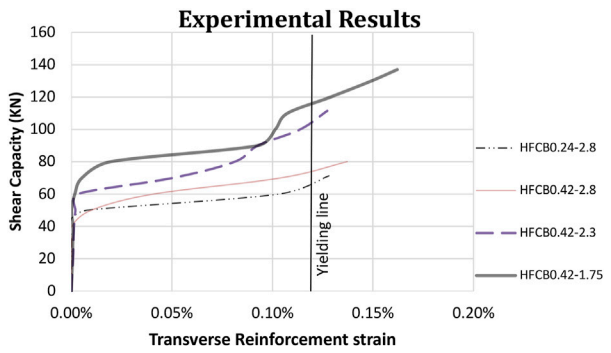

FIGURE 7
The relation between load and strain at transverse reinforcement for concrete beams HFCB0.24-2.8, HFCB0.42-2.8, HFCB0.42-2.3, and HFCB0.42-1.75.

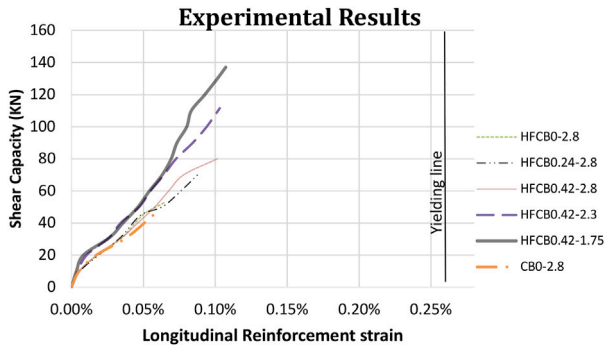

FIGURE 8
The relation between load and strain at longitudinal reinforcement for all concrete beams.

and transverse steel reinforcement to delay the cracking process, improve stiffness and strength, and reduce deformation values at the same load. Adding hybrid fibers, increasing the transverse reinforcement ratio, as well as decreasing the span to depth ratio resulted in a decrease in the deflection values at the same load, due to the delay in the cracking process, which improved stiffness and strength and ultimately showed lower deformation values. However, the decrease in span to depth ratio reduced the ductility of the beam to the point where it could not be inelastically deformed without failure. The highest maximum deformation was reported in the hybrid FRC beam HFCB0.42-2.8, which contains transverse steel reinforcement and hybrid fibers. This demonstrates the significance of both hybrid fibers and transverse reinforcement in lowering the brittleness of concrete and enhancing its ability for plastic deformation without fracture (Khan et al., 2021a; Khan et al., 2021b; Abbas et al., 2022; Abbas and Khan, 2022).

3.2.2 Load versus strain of transverse reinforcement all concrete beams

The relationship between load and strain values in transverse steel reinforcement for hybrid FRC beams that contain transverse reinforcement is illustrated in Figure 7. The strain values in the transverse reinforcement at the crack load were .003%, .0012%, .002%, and .0017% For the concrete beams HFCB0.24-2.8, HFCB0.42-2.8, HFCB0.42-2.3, and HFCB0.42-1.75 respectively. While the strain values at failure load for the concrete beams HFCB0.24-2.8, HFCB0.42-2.8, HFCB0.42-2.3, and HFCB0.42-1.75 were .13%, .14%, .13%, and .16%, respectively. The findings demonstrate that the strain values in the transverse reinforcement were insignificant at the initial shear crack but significantly increased with increasing loading until they reached yield for all concrete beams that contain transverse reinforcement, explaining the occurrence of severe diagonal shear cracks at collapse.

3.2.3 Load versus strain of longitudinal reinforcement all concrete beams

Figure 8 shows the relationship between load and strain values in longitudinal steel reinforcement for all concrete beams. For the concrete beams CB0-2.8, HFCB0-2.8, HFCB0.24-2.8, HFCB0.42-2.8, HFCB0.42-2.3, and HFCB0.42-1.75, the strain values in the longitudinal reinforcement at the crack load were .017%, .018%, .034%, .045%, .047%, and .054%, respectively. Whereas for the concrete beams CB0-2.8, HFCB0-2.8, HFCB0.24-2.8, HFCB0.42-2.8, HFCB0.42-2.3, and HFCB0.42-1.75, the longitudinal reinforcement strain values at failure load were .06%, .07%, .09%, .1%, .1%, and .11%, respectively. The results show that the longitudinal reinforcement strain did not reach yield for all concrete specimens, indicating that flexure stresses were insufficient to affect the failure mode, which was controlled by shear stresses.

4 Discussion

4.1 Cracking pattern and failure mode

Figure 9 shows the failure mode for all concrete beam specimens. Vertical cracks appeared in the flexure region for control beam CB0-2.8 which does not contain fibers, and then a single diagonal tension crack due to shear appeared in the shear region at the bottom and spread upwards with the increase in loading until it reached the location of the load's impact, and then a brittle collapse occurred as a result of a widening diagonal shear crack, recognizing that the beam collapsed shortly after the initiation of diagonal shear cracks, indicating low ductility. Also, just before failure, spalling was observed

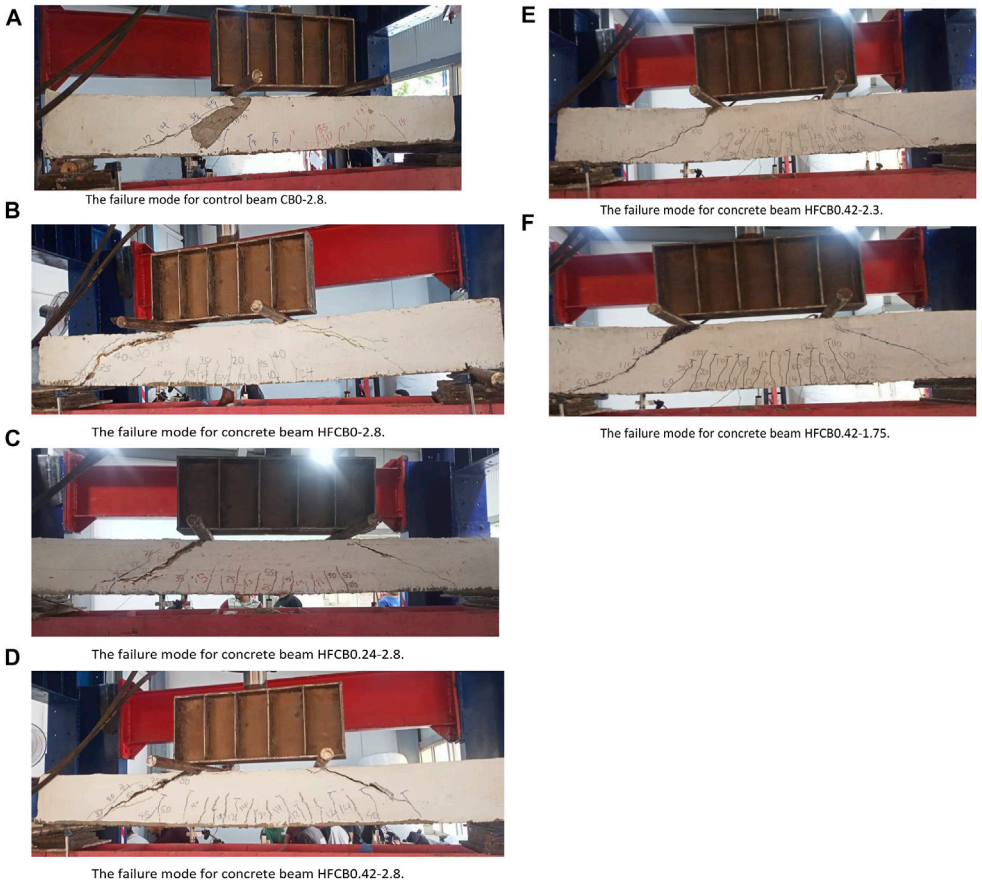

FIGURE 9
Failure modes for all concrete beams. **(A)** The failure mode for control beam CB0-2.8. **(B)** The failure mode for concrete beam HFCB0-2.8. **(C)** The failure mode for concrete beam HFCB0.24-2.8. **(D)** The failure mode for concrete beam HFCB0.42-2.8. **(E)** The failure mode for concrete beam HFCB0.42-2.3. **(F)** The failure mode for concrete beam HFCB0.42-1.75.

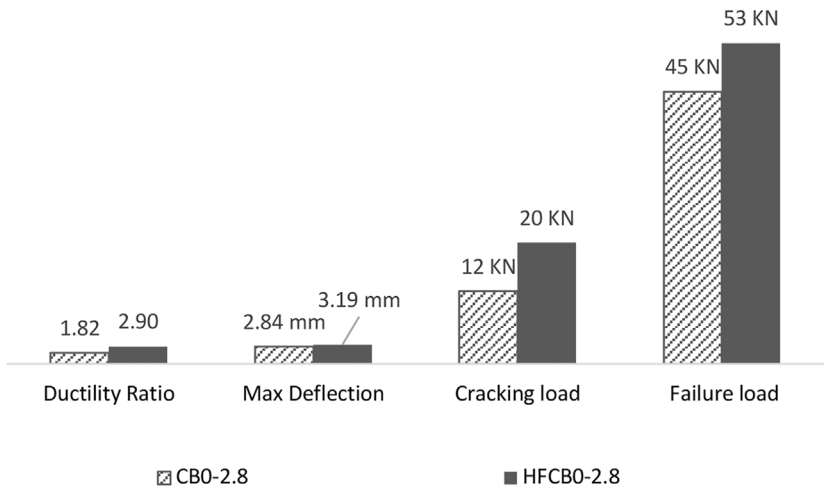

FIGURE 10
Effect of using hybrid polypropylene-steel fibers.

on the external surface of the concrete beam at the compression zone and extended along with the diagonal crack, indicating that the applied stresses exceeded the compressive strength of the concrete. The hybrid FRC beam HFCB0-2.8 failed due to the widening of a diagonal shear crack. The first diagonal shear crack for hybrid FRC beam HFCB0-2.8 appeared at a load of 20 kN

TABLE 6 Analysis of all concrete beams.

Beam ID	$\frac{V_{failure\ for\ HFCB}}{V_{failure\ for\ CB}}$	$\frac{V_{cracking\ for\ HFCB}}{V_{cracking\ for\ CB}}$	$\frac{\Delta_{max\ for\ HFCB}}{\Delta_{max\ for\ CB}}$	$\frac{Ductility\ for\ HFCB}{Ductility\ for\ CB}$
CB0-2.8	—	—	—	—
HFCB0-2.8	1.18	1.66	1.13	1.60
HFCB0.24-2.8	1.58	2.58	1.37	1.77
HFCB0.42-2.8	1.78	3.08	1.45	2.07
HFCB0.42-2.3	2.48	4.33	1.69	1.46
HFCB0.42-1.75	3.04	5.00	1.42	1.27

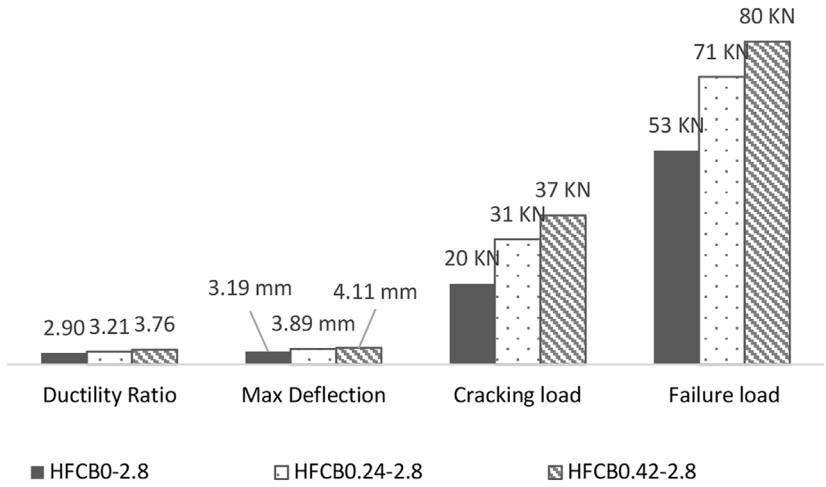

FIGURE 11
Effect of using transverse reinforcement.

while it appeared at a load of 12 kN for the control beam, demonstrating the significance of fibers in preventing crack initiation and propagation. More shear and flexure cracks appeared for the hybrid FRC beam HFCB0-2.8 than in the control beam due to the presence of fibers which prevents cracks from widening and spreading, causing high tensile stresses to be transmitted from the location of the existing cracks to the region between them. This leads to the development of new cracks, increasing the total number of cracks (Tahenni et al., 2016; Alrefaei et al., 2018; Shaaban et al., 2021). Hybrid FRC beam HFCB0-2.8 did not experience significant concrete spalling because the fibers improved the stiffness and strength. When transverse reinforcement was added to the prior hybrid FRC beam, the failure mechanism remained the same as the diagonal shear crack caused the collapse of the hybrid FRC beams HFCB0.24-2.8 and HFCB0.42-2.8. However, increasing the transverse reinforcement ratio resulted in higher shear strength, a slower rate of shear cracking, and more cracks, demonstrating the effectiveness of adding transverse reinforcement in delaying the cracking process and enhancing concrete's ductility, stiffness, and shear strength. The failure for both hybrid FRC beams HFCB0.42-2.3 and HFCB0.42-1.75 occurred due to diagonal shear cracks and was followed by crushing of concrete in the compression zone.

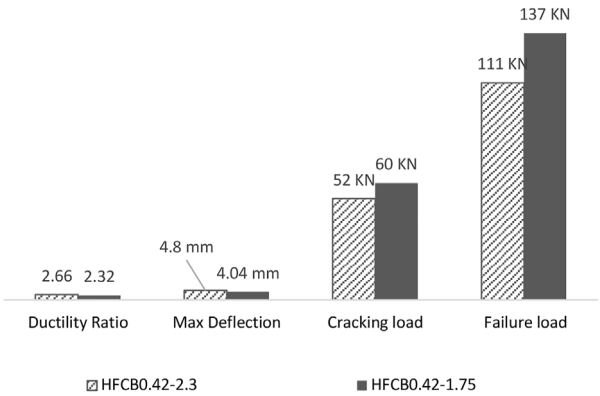

FIGURE 12
Effect of span to depth ratio.

However the shear crack width decreased, and the shear strength was noticeably improved for concrete beam HFCB0.42-1.75 more than the concrete beam HFCB0.42-2.3. This is due to a substantial proportion of the shear being immediately transferred to the support *via* an inclined strut. The direct load transfer's magnitude develops with a lowering span to depth ratio and

TABLE 7 Hybrid FRC properties.

Material model	Element type	Modulus of elasticity (GPa)	Poisson's ratio	Uniaxial crushing (MPa)	Uniaxial cracking (MPa)	Open shear coefficient	Close shear coefficient
1	Solid65	38	.2	60	5.5	.5	1

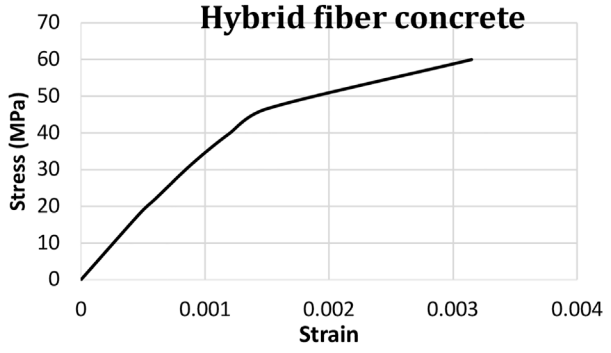

FIGURE 13
Stress-strain curve for hybrid fiber concrete.

has been known as the arch action mechanism (Ali et al., 2021; Ebid and Deifalla, 2021; Deifalla, 2021b; Li et al., 2021; Deifalla and Mukhtar, 2022a; Deifalla and Mukhtar, 2022b; Zhou and Wan, 2022). This mechanism inhibits cracks from growing larger and delays stirrup yielding. Additionally, it was observed that flexural cracks began growing larger and deeper as the span-to-depth ratio decreased. This refers to an increase in the tensile stresses caused by flexure in addition to the strain of the longitudinal reinforcement, however, the failure mode remained diagonal shear failure and did not transform for being combined shear-flexure or flexure failure since the longitudinal steel bars had not yet reached yielding.

4.2 Effect of using hybrid polypropylene-steel fibers

The use of hybrid polypropylene-steel fibers improved ultimate and cracking shear strength, as well as ductility, in concrete beams. As shown in Figure 10, the values of ultimate shear load, cracking shear load, maximum deformation, and ductility for hybrid FRC beam HFCB0-2.8 increased by 18%, 66%, 13%, and 60%, respectively, over the control beam CB0-2.8. Ductility is the ability of concrete to plastically deform without fracturing when subjected to tensile stress greater than its strength. It can be computed by dividing the ultimate deformation that occurs at the ultimate shear force by the cracking deformation that occurs at the cracking shear force (Pakravan et al., 2016; Yan et al., 2021). The fact that when the hybrid fibers were added, the cracking and ultimate shear strengths increased supports their ability to withstand macro and micro cracks at different stress levels, delaying the cracking process and improving stiffness and strength (Tahenni et al., 2016; Sivakumar et al., 2020; Ismail and Hassan, 2021; Shaaban et al., 2021; Yang et al., 2021; Tawfik et al., 2022). The increase in ultimate deformation and ductility values is a further indication of the efficacy of hybrid fibers in reducing concrete's brittleness and improving its capability for plastic deformation without fracture. Table 6 illustrates the analysis of shear failure load, shear cracking load, maximum deformation, and ductility results for all concrete beams.

4.3 Effect of using transverse reinforcement

Transverse reinforcement improved ultimate shear strength, cracking behavior, and ductility in concrete beams as shown in Figure 11. In comparison to the hybrid FRC beam HFCB0-2.8, the values of ultimate shear load, cracking shear load, maximum deformation, and ductility for hybrid FRC beam HFCB0.42-2.8 improved by 35%, 55%, 22%, and 11%, respectively. Additionally, the values of the ultimate shear load, cracking shear load, maximum deformation, and ductility increased by 12%, 19%, 6%, and 17%, respectively, as the transverse reinforcement ratio increased from .24% to .42%. Transverse steel reinforcement, which is similar to hybrid fibers, could postpone shear cracking while simultaneously enhancing shear strength and ductility (Alrefaei et al., 2018; Torres and Lantsoght, 2019; Yang et al., 2021).

4.4 Effect of span to depth ratio

As shown in Figure 12, the ultimate shear load and cracking shear load for hybrid FRC beam HFCB0.42-1.75, which has a span to depth ratio of 1.75 improved by 23% and 15%, respectively, more than for hybrid FRC beam HFCB0.42-2.3, which has a span to depth ratio of 2.3, and by 71% and 62%, respectively, more than for hybrid FRC beam HFCB0.42-2.8, which has a span to depth ratio of 2.8. These findings support the fact that lowering the span-to-depth ratio greatly improves shear strength because a considerable

TABLE 8 Transverse and longitudinal steel properties.

	Material model	Element type	Modulus of elasticity (GPa)	Poisson's ratio	Yield stress (MPa)
Longitudinal steel bars	2	Link180	200	.3	520
Transverse steel bars	3	Link180	200	.3	240

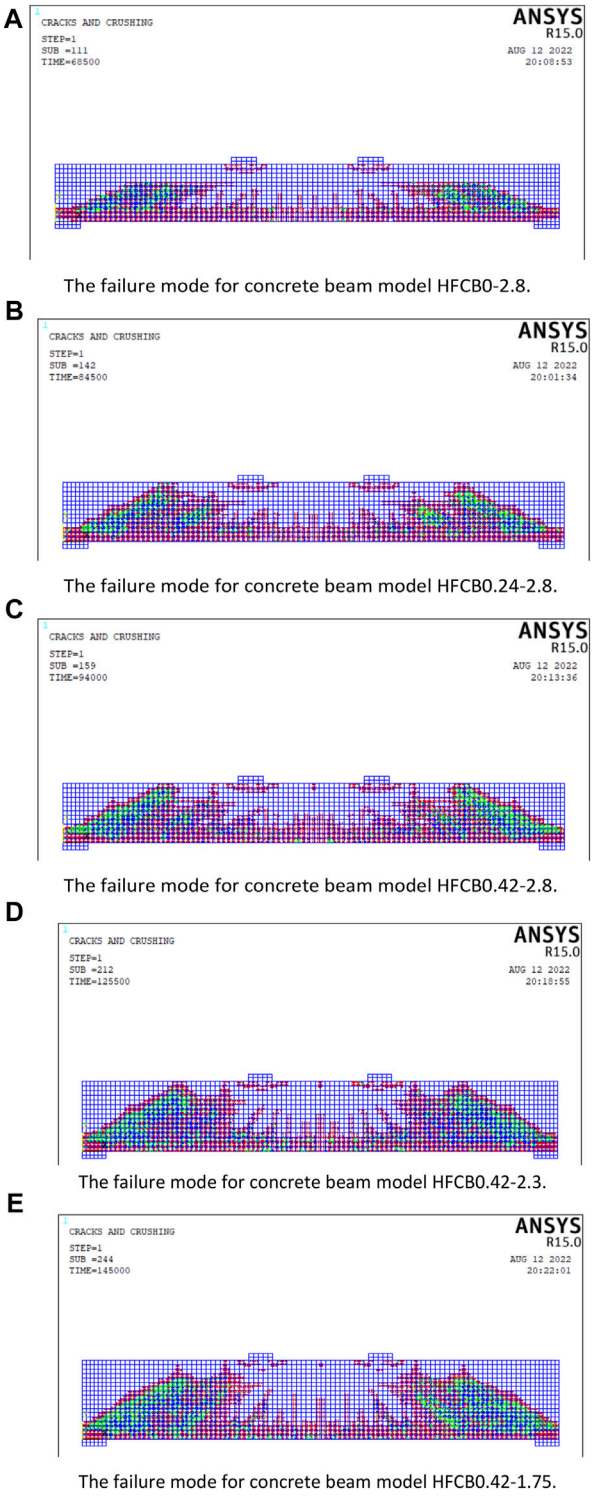

FIGURE 14
Failure modes for all hybrid FRC beam models. **(A)** The failure mode for concrete beam model HFCB0-2.8. **(B)** The failure mode for concrete beam model HFCB0.24-2.8. **(C)** The failure mode for concrete beam model HFCB0.42-2.8. **(D)** The failure mode for concrete beam model HFCB0.42-2.3. **(E)** The failure mode for concrete beam model HFCB0.42-1.75.

percentage of the shear force is transferred directly to the support by an inclined strut (arch action mechanism). This mechanism slows down the cracking process while enhancing stiffness and shear strength, which results in minor deformation occurring under the same load. In contrast, the hybrid FRC beam HFCB0.42-1.75, which has a span to depth ratio of 1.75, displayed the lowest deformation values at the same load and ductility, where they decreased by 16% and 13%, respectively,

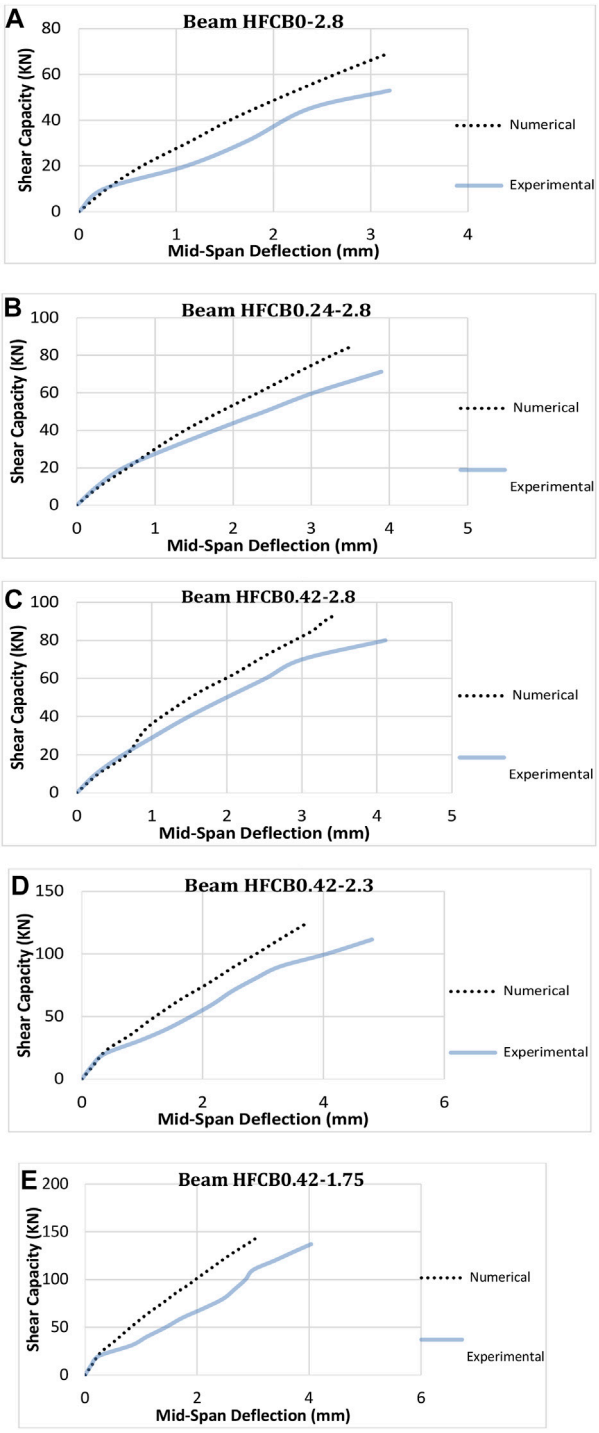

FIGURE 15
Experimental and numerical load-deflection curves for all hybrid FRC beams: **(A)** HFCB0-2.8, **(B)** HFCB0.24-2.8, **(C)** HFCB0.42-2.8, **(D)** HFCB0.42-2.3, and **(E)** HFCB0.42-1.75.

more than for the hybrid FRC beam HFCB0.42-2.3, which has a span to depth ratio of 2.3, and by 2% and 38%, respectively, more than for the hybrid FRC beam HFCB0.42-2.8, which has a span to depth ratio of 2.8. This indicates that although lowering the span to depth ratio increases the concrete's shear strength, it has a detrimental effect on the ductility because the concrete beam was unable to withstand inelastic deformation and collapsed suddenly once the first diagonal shear crack appeared.

5 Finite element model

ANSYS 15 software is used to produce a numerical model, which is then validated with experimental results. A total of five finite element models that accurately represent the experimental HPSFRC beams HFCB0-2.8, HFCB0.24-2.8, HFCB0.42-2.8, HFCB0.42-2.3, and HFCB0.42-1.75 were created.

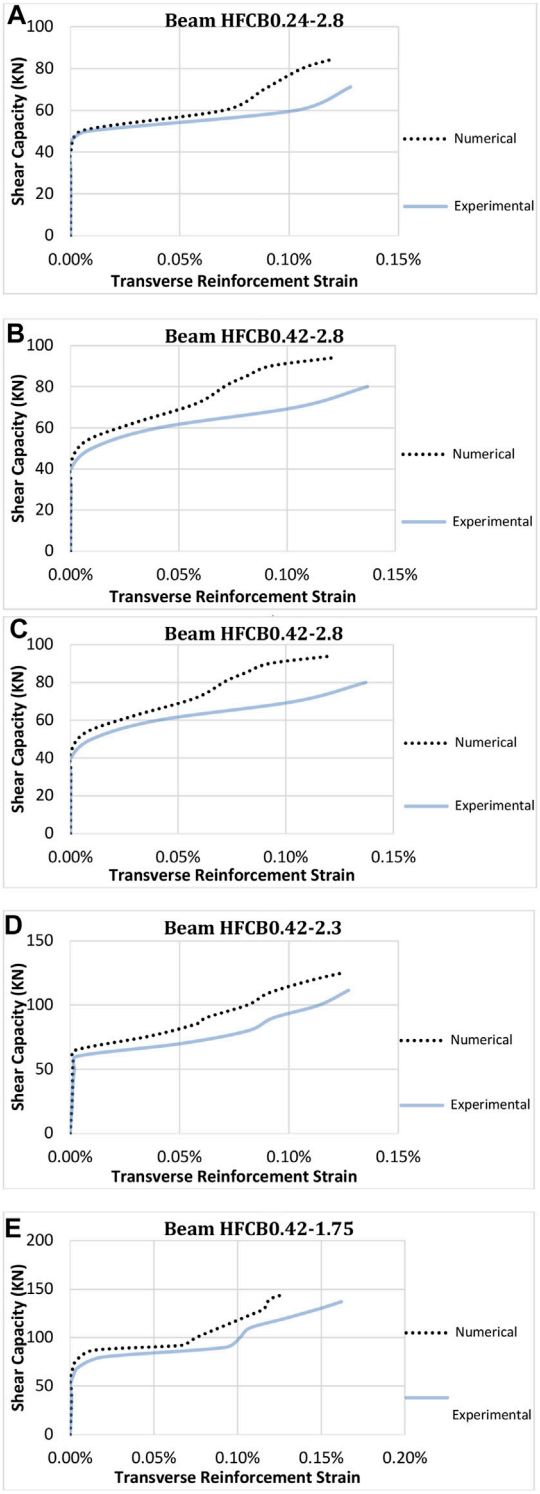

FIGURE 16
Experimental and numerical load-transverse reinforcement strain curves for all hybrid FRC beams: **(A)** HFCB0-2.8, **(B)** HFCB0.24-2.8, **(C)** HFCB0.42-2.8, **(D)** HFCB0.42-2.3, and **(E)** HFCB0.42-1.75.

5.1 Materials, loads, and boundary conditions modelling

The defined parameters of the concrete are shown in Table 7 and include the elastic modulus, Poisson's ratio, uniaxial crushing, uniaxial cracking, open shear, and close shear coefficient. The non-linear behavior of hybrid FRC beams was modeled using the stress-strain relationship shown in Figure 13, which was derived from the result of the uniaxial confined compressive strength test. Shear transfer coefficients are typically measured in the range of .0–1.0, with

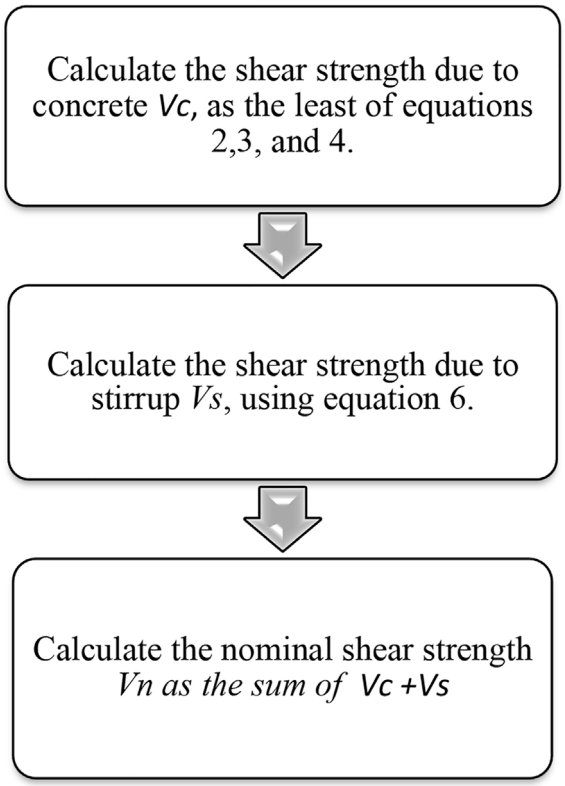

FIGURE 17
Flow chart for shear strength calculation using ACI.

.0 denoting a smooth crack (total loss of shear transfer) and 1.0 denoting a rough crack (no loss of shear transfer). According to (Tahenni et al., 2021), the shear transfer coefficient for open and closed fractures was estimated, and the results were reasonably close to the experimental results. The longitudinal and transverse reinforcements were modeled using the Link 180 element. Table 8 represents the inserted properties of the transverse and longitudinal reinforcements including modulus of elasticity, Poisson's ratio, and yield stress. The non-linear behaviors of transverse and longitudinal reinforcements were modeled based on the tensile test results. At a distance of 700 mm from the support on either side, double lines of nodes on the upper steel plates are where the force is acting. Two lines of nodes on the bottom end of the beam represent the hinged and roller supports. The roller support was restricted from moving in Y-direction, while the hinged support was restricted from moving in both X, Y, and Z-directions. The steel plates were represented by Link185 element.

5.2 Numerical analysis procedure

The software performs a linear solution for the numerical simulations, gradually increasing the load value, and analyzing convergence. When the requirements are not met, various solution is developed by modifying the stiffness matrix. Collapse can be recognized by cracking patterns, concrete compressive strain approaching maximum, steel reinforcing strain reaching yield, or non-convergence resulting from a total loss of load-bearing capacity. The convergence criteria throughout the current investigation were dependent on force and displacement.

5.3 Validation of the numerical models

The finite element and experimental outputs were compared to validate the experimental findings. This was accomplished to guarantee that the concrete beam's convergence conditions are suitable. Figure 14 illustrates the crack patterns and failure modes of hybrid FRC beams based on finite element models. All finite element models cracked similarly to all concrete beams in the experimental program. Where flexural cracks first appeared at the flexure region, followed by shear-flexure cracks, and finally diagonal shear cracks initiated and propagated upward at a 45-degree angle towards the applied load until the beams failed. The failure mode of the finite element model HFCB0-2.8 was similar to that of its experimental equivalent, where diagonal shear cracks occurred, followed by stirrup yielding, which caused the collapse. The finite element model differs in that the diagonal shear crack did not extend to the point where the load was impacting. This is likely because the stirrup reached yield stress before the diagonal shear crack was fully completed. This shows that the finite element model did not exhibit the same level of ductility as in the experimental beam sample to allow for the formation of a full diagonal crack before the collapse, but the failure mode is still the same for both as a diagonal shear crack followed by stirrup yielding. Regarding the finite element model HFCB0.24-2.8, the shown failure mode demonstrated that the addition of stirrups improved its ductility in such a way that it resulted in the formation

TABLE 9 Experimental, numerical, and ACI, results of shear failure load for all beams.

Mix ID	Shear failure load V(kN)			$\frac{V_{Exp}}{V_{Num}}$	$\frac{V_{Exp}}{V_{ACI}}$	$\frac{V_{Num}}{V_{ACI}}$
	V_{Exp}	V_{Num}	V_{ACI}			
HFCB0-2.8	53	68.5	40.6	.77	1.30	1.69
HFCB0.24-2.8	71	84.5	56.2	.84	1.27	1.50
HFCB0.42-2.8	80	94	68.3	.85	1.17	1.38
HFCB0.42-2.3	111	125.5	83.2	.89	1.34	1.51
HFCB0.42-1.75	137	145	112.9	.94	1.21	1.28
Average				.86	1.26	1.47
Standard deviation				.056	.061	.136
Coefficient of variance %				6.5	4.8	9.2

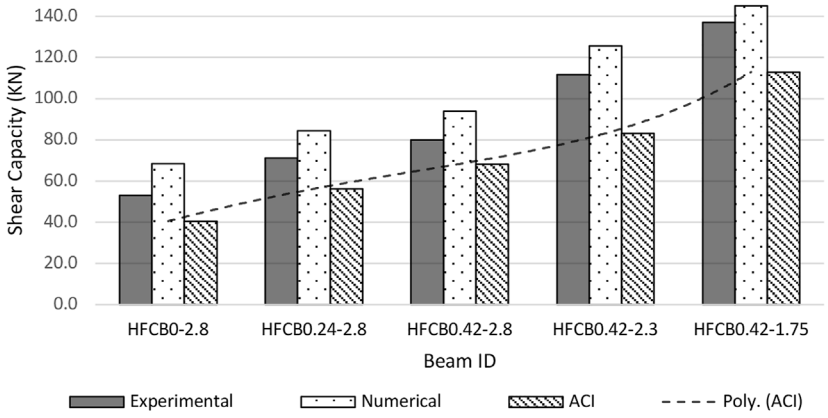

FIGURE 18
Comparison between the experimental, numerical, and ACI results of shear failure load for all concrete beams.

of a full diagonal shear crack from the support up to the upper edge, followed by the stirrup yielding, which was very similar failure behavior to that experimental equivalent. The failure mode for finite element model HFCB0.42-2.8 did not differ significantly from finite element model HFCB0.24-2.8, as the collapse occurred as a result of a full diagonal shear crack occurring and the stirrups reached yield except with clearer shear-flexure cracks, because the beam could bear higher loads and thus the flexure stresses increased, and consequently, the flexure cracks increased, however, this was ineffective in changing the failure mode. The failure mode and crack pattern for finite element model HFCB0.42-2.8 were very similar to the corresponding experimental sample. The failure mode of finite element model HFCB0.24-2.3 was very similar to that of finite element model HFCB0.24-2.8, but with more and clearer flexural cracks since the strength of the beam increased as the span to depth ratio decreased, and thus the flexure stresses and flexure cracks increased. This failure and crack pattern were quite similar to the equivalent experimental beam. The failure mode of finite element model HFCB0.42-1.75 was comparable to that of the corresponding experimental beam model, except that the diagonal shear crack did not reach the top edge. This confirms that decreasing the span to depth ratio reduced the ductility of the beam, and thus the stirrup reached yield before a complete diagonal shear crack occurred. Additionally, the experimental one had more concrete crushing at the compression zone although this had no effect on the collapse because it was governed by the diagonal shear crack followed by stirrup yielding. Figure 15 shows a comparison between the finite element and experimental load versus deflection curves for all concrete beams. The finite element failure load was higher than the experimental failure load by 29%, 19%, 18%, 13%, and 6% for hybrid reinforced concrete beams HFCB0-2.8, HFCB0.24-2.8, HFCB0.42-2.8, HFCB0.42-2.3, and HFCB0.42-1.75, respectively. The coefficient of variance between the finite element and the experimental results of failure load was 6.5%. The deflection values of all finite element and experimental samples appeared to be nearly equal as shown in the figure, and the relationship between load and deflection seemed to be linear until the crack occurs. Following the occurrence of the crack, the relationship became non-linear with an increase in the experimental sample's deflection values compared to the finite element model at the same load. The finite element maximum deflection was 2%, 10%, 16%, 22%, and 23% less than the experimental maximum deflection for hybrid reinforced concrete beams HFCB0-2.8, HFCB0.24-2.8, HFCB0.42-2.8, HFCB0.42-2.3, and HFCB0.42-1.75, respectively. The maximum deflection experimental results and the finite element results have a 9% coefficient of variation. Figure 16 compares the finite element

and experimental load-transverse strain curves for all concrete beams. The strain values in stirrups for all finite element and experimental samples were insignificant until the cracking load. Following that, the strain in the stirrups increased dramatically until it reached yield stress. The figure shows that the strain values for the experimental samples after the cracking load were greater than the strain values for the finite element models under the same load. For all experimental and finite element models, the strain in the stirrups reached yield. The finite element transverse reinforcement strain values at failure were 15%, 6%, 12%, 1%, and 2% lower for the hybrid reinforced concrete beams HFCB0-2.8, HFCB0.24-2.8, HFCB0.42-2.8, HFCB0.42-2.3, and HFCB0.42-1.75, respectively compared to the experimental transverse reinforcement strain values at failure. Transverse reinforcement strain experimental results and the results from the finite element had a 7.3% coefficient of variation. The comparison revealed that the experimental and finite element results were perfectly correlated.

6 Comparison with ACI

The shear strength for hybrid polypropylene-steel fibers reinforced concrete beams was calculated in this section using ACI provisions. The validation of the finite element and experimental results are demonstrated by comparing them to the ACI equations. As illustrated in Figure 17, the nominal shear strength *Vn* can be calculated as the summation of the nominal shear strength due to concrete *Vc*, and the nominal shear strength due to transverse reinforcement Vs. According to ACI318 (ACI 318-19, 2019), the nominal shear strength due to concrete can be calculated as the least of the followings:

$$V_c = 0.17\lambda \sqrt{f_c'}\, b_w d \tag{2}$$

$$V_c = 0.66\lambda\, \rho^{1/3} \sqrt{f_c'}\, b_w d \tag{3}$$

$$V_c = 0.42\lambda \sqrt{f_c'}\, b_w d \tag{4}$$

λ is the reduction factor equal to one for normal weight concrete as well as high strength concrete. f_c' is the cylindrical compressive strength of concrete. ρ is the ratio of the area of longitudinal reinforcement to the cross-section of the concrete area $b_w d$.

The correction factor for obtaining the equivalent compressive strength of the standard cube is given by ECP203 (ECP 203-18, 2018) as follows:

$$f_{cu} = 1.25\, f_c' \tag{5}$$

Where f_{cu} is the cubic ultimate compressive strength of concrete.

The nominal shear strength due to transverse reinforcement is calculated as the following:

$$V_s = \frac{A_v f_y}{s} d \tag{6}$$

A_v is the area of transverse reinforcement. f_y is the yield strength of transverse reinforcement. ρ is the spacing between the transverse reinforcement.

Table 9 shows a comparison between the numerical, experimental, and ACI predicted values of shear strength for hybrid polypropylene-steel fibers reinforced concrete beams. ACI results exhibited the lowest values of shear capacity for all hybrid FRC beams while the numerical exhibited the largest values. As shown in Figure 18, the ACI results for shear capacity were less than the experimental results by 23%, 21%, 15%, 25%, and 18% for concrete beams HFCB0-2.8, HFCB0.24-2.8, HFCB0.42-2.8, HFCB0.42-2.3, and HFCB0.42-1.75, respectively. On the other hand, the ACI results for shear capacity were less than the numerical results by 41%, 33%, 27%, 34%, and 22% for concrete beams HFCB0-2.8, HFCB0.24-2.8, HFCB0.42-2.8, HFCB0.42-2.3, and HFCB0.42-1.75, respectively. The coefficient of variance between the ACI and experimental shear capacity results was 4.8%, while it was 9.2% between the ACI and numerical shear capacity results. This indicates that the shear capacity of hybrid polypropylene-steel fibers reinforced concrete beams predicted by ACI is appropriate, However, the ACI underestimated shear strength. The ACI's calculations were conservative when compared with the experimental or numerical results, particularly for hybrid FRC beams with a lower transverse reinforcement ratio or a lower span-to-depth ratio (equal or less than 2.3).

7 Conclusion

The shear behavior of concrete elements is a dilemma. This study examined the shear behavior of high-strength concrete beams reinforced with hybrid polypropylene-steel fibers. Concrete type, transverse reinforcement ratio, and span to depth ratio were the investigated parameters that influenced the shear behavior. The following crucial findings were condensed from the theoretical and practical study:

1. Experimental HFRHSC beams with a span-to-depth ratio larger than 2.3 failed due to a significant diagonal shear crack, whereas concrete beams with a span-to-depth ratio equal to or less than 2.3 failed due to a diagonal shear crack followed by crushing of concrete. This is because decreasing the span-to-depth ratio changed the shear resistance behavior from truss to arch action, and thus the failure was controlled more by the compressive strength of inclined struts.
2. Adding hybrid polypropylene-steel fibers to high-strength concrete beams improved shear capacity, maximum deformation, and ductility, as well as delayed crack initiation by approximately 18%, 66%, 60%, and 13%, respectively. This is due to the capability of hybrid polypropylene-steel fibers to withstand macro and micro cracks at different stress levels, thus delaying the cracking process, improving stiffness and strength, reducing brittleness, and increasing plastic deformation without fracture.
3. Adding transverse reinforcement to high-strength concrete beams alongside hybrid polypropylene-steel fibers and longitudinal reinforcement at the compression zone improved the ability to prevent crack initiation and propagation, as well as increased the shear strength and ductility more than adding hybrid fibers alone, where the shear capacity, the cracking load, maximum deformation, and ductility for hybrid fiber reinforced high-strength concrete beams that had transverse reinforcement, were 35%, 55%, 22%, and 11% higher, respectively than those for hybrid fiber reinforced high-strength concrete beam without transverse reinforcement.
4. Reducing the span-to-depth ratio for HFRHSC beams from 2.8 to 1.75 increased shear capacity and cracking load by about 22% and 11%, respectively, however, decreased maximum deformation and ductility by about 2% and 38%, respectively. This is because the load was transmitted directly to the support with a decrease in the span-to-depth ratio, which delayed the occurrence of cracking and improved

shear strength while negatively affecting the ability to plastically deform and ductility, making concrete behave more brittle.
5. The numerical results for HFRHSC beams modeled with ANSYS 15 software showed a good correlation with the experimental results; however, the numerical solution overestimated the shear capacity. The average and coefficient of variance between the experimental and numerical results for shear capacity were .86% and 6.5%, respectively.
6. The ACI's calculations were conservative when compared with the experimental or numerical results, particularly for hybrid fiber-reinforced high-strength concrete beams with a lower transverse reinforcement ratio or a lower span-to-depth ratio. The coefficient of variance between the ACI and experimental shear capacity results was 4.8%, while it was 9.2% between the ACI and numerical shear capacity results.

8 Future studies

1. Studying the effect of different span-to-depth ratios (1, 1.5, 3, 4) on the shear behavior of HFRHSC beams.
2. Studying the effect of different proportions of hybrid polypropylene-steel fibers (10%, 15%, 20%, 25%) on the shear behavior of high-strength concrete beams.
3. Studying the effect of flange width for L-section and T-section on the shear behavior of HFRHSC beams.
4. Studying the flexural behavior of HFRHSC beams.
5. Studying the torsional behavior of HFRHSC beams.

Data availability statement

The original contributions presented in the study are included in the article/supplementary material, further inquiries can be directed to the corresponding authors.

Author contributions

Conceptualization, MS and AA; methodology, MT, MA, and MS; software and investigation, MT; validation, AD; formal analysis, AA and MA; resources and data curation, AE-s; writing—original draft preparation, AA and AD; writing—review and editing, MA and MS; visualization, AD; supervision, MS and AD; funding acquisition, MS. All authors have read and agreed to the published version of the manuscript.

Funding

The research is partially funded by the Ministry of Science and Higher Education of the Russian Federation under the strategic academic leadership program "Priority 2030" (Agreement 075-15-2021-1333, dated 30 September 2021).

Conflict of interest

The authors declare that the research was conducted in the absence of any commercial or financial relationships that could be construed as a potential conflict of interest.

Publisher's note

All claims expressed in this article are solely those of the authors and do not necessarily represent those of their affiliated organizations, or those of the publisher, the editors and the reviewers. Any product that may be evaluated in this article, or claim that may be made by its manufacturer, is not guaranteed or endorsed by the publisher.

References

Abbas, W., and Khan, M. I. (2022). Experimental and numerical investigation of flexural behavior of hybrid fiber reinforced high strength incorporating binary and ternary blend of ultra fines. *Structures* 42, 53–64. doi:10.1016/j.istruc.2022.05.116

Abbas, Y. M., Hussain, L. A., and Khan, M. I. (2022). Constitutive compressive stress–strain behavior of hybrid steel-PVA high-performance fiber-reinforced concrete. *J. Mater. Civ. Eng.* 34. doi:10.1061/(ASCE)MT.1943-5533.0004041

ACI 318-19 (2019). *Building code requirements for structural concrete and commentary*. Farmington Hills, MI 48331, U.S.A.: American Concrete Institute. 2014.

Ahmad, J., Majdi, A., Al-Fakih, A., Deifalla, A. F., Althoey, F., El Ouni, M. H., et al. (2022). Mechanical and durability performance of coconut fiber reinforced concrete: A state-of-the-art review. *Materials* 15, 3601. doi:10.3390/ma15103601

Ahmed, A., Abbas, S., Abbass, W., Waheed, A., Razzaq, A., Ali, E., et al. (2022). Potential of waste marble sludge for repressing alkali-silica reaction in concrete with reactive aggregates. *Materials* 15, 3962. doi:10.3390/ma15113962

Ali, B., Kurda, R., Herki, B., Alyousef, R., Mustafa, R., Mohammed, A., et al. (2020). Effect of varying steel fiber content on strength and permeability characteristics of high strength concrete with micro silica. *Materials* 13, 5739. doi:10.3390/ma13245739

Ali, A., Hamady, M., Chalioris, C. E., and Deifalla, A. (2021). Evaluation of the shear design equations of FRP-reinforced concrete beams without shear reinforcement. *Eng. Struct.* 235, 112017. doi:10.1016/j.engstruct.2021.112017

Ali, B., Fahad, M., Ullah, S., Ahmed, H., Alyousef, R., and Deifalla, A. (2022). Development of ductile and durable high strength concrete (HSC) through interactive incorporation of coir waste and silica fume. *Materials* 15, 2616. doi:10.3390/ma15072616

Alrefaei, Y., Rahal, K., and Maalej, M. (2018). Shear strength of beams made using hybrid fiber-engineered cementitious composites. *J. Struct. Eng.* 144. doi:10.1061/(ASCE)ST.1943-541X.0001924

Ashraf, M. R., Akmal, U., Khurram, N., Aslam, F., and Deifalla, A. F. (2022). Impact resistance of styrene–butadiene rubber (SBR) latex-modified fiber-reinforced concrete: The role of aggregate size. *Materials* 15, 1283. doi:10.3390/ma15041283

Ayub, T., Khan, S. U., and Ayub, A. (2019). Analytical model for the compressive stress–strain behavior of PVA-FRC. *Constr. Build. Mater* 214, 581–593. doi:10.1016/j.conbuildmat.2019.04.126

Deifalla, A. F., Zapris, A. G., and Chalioris, C. E. (2021). Multivariable regression strength model for steel fiber-reinforced concrete beams under torsion. *Materials* 14, 3889. doi:10.3390/ma14143889

Deifalla, A. (2021a). Refining the torsion design of fibered concrete beams reinforced with FRP using multi-variable non-linear regression analysis for experimental results. *Eng. Struct.* 224, 111394. doi:10.1016/j.engstruct.2020.111394

Deifalla, A. (2021b). Assessment of one-way shear design of RC elements subjected to axial tension. *Case Stud. Constr. Mater.* 15, e00620. doi:10.1016/j.cscm.2021.e00620

Deifalla, A. F., and Mukhtar, F. M. (2022). Shear strength of lightweight and normal-weight concrete slender beams and slabs: An appraisal of design codes. *Adv. Struct. Eng.* 25, 2444–2466. doi:10.1177/13694332221098869

Deifalla, A., and Mukhtar, F. M. (2022). A mechanical and simplified model for RC elements subjected to combined shear and axial tension. *Sci. Rep.* 12, 7863. doi:10.1038/s41598-022-11577-y

Ebid, A., and Deifalla, A. (2021). Prediction of shear strength of FRP reinforced beams with and without stirrups using (GP) technique. *Ain Shams Eng. J.* 12 (3), 2493–2510. doi:10.1016/j.asej.2021.02.006

ECP 203-18 (2018). *Egyptian code for design and construction of concrete buildings"*. Cairo, Egypt: National Center for Research.

Fadil, D., Taysi, N., and Ahmed, A. (2018). *The investigation of basalt and glass Fibers on the behavior of reinforced concrete beams*. Available at: http://iraj.in (Accessed July 31, 2019).

Ghareeb, K. S., Ahmed, H. E., El-Affandy, T. H., Deifalla, A. F., and El-Sayed, T. A. (2022). The novelty of using glass powder and lime powder for producing UHPSCC. *Buildings* 12, 684. doi:10.3390/buildings12050684

Hoang, A. L., and Fehling, E. (2017). Influence of steel fiber content and aspect ratio on the uniaxial tensile and compressive behavior of ultra-high-performance concrete. *Constr. Build. Mat.* 153, 790–806. doi:10.1016/j.conbuildmat.2017.07.130

Huang, S., Wang, H., Ahmad, W., Ahmad, A., Ivanovich Vatin, N., Mohamed, A. M., et al. (2022). Plastic waste management strategies and their environmental aspects: A scientometric analysis and comprehensive review. *Int. J. Environ. Res. Public Health* 19, 4556. doi:10.3390/ijerph19084556

Ismail, M. K., and Hassan, A. A. (2021). Influence of fibre type on the shear behaviour of engineered cementitious composite beams. *Mag. Concr. Res.* 73 (9), 464–475. doi:10.1680/jmacr.19.00172

Juenger, M. C. G., Snellings, R., and Bernal, S. A. (2019). Supplementary cementitious materials: New sources, characterization, and performance insights. *Cem. Concr. Res.* 122, 257–273. doi:10.1016/j.cemconres.2019.05.008

Khan, M., Cao, M., and Ali, M. (2020). Cracking behaviour and constitutive modelling of hybrid fibre reinforced concrete. *J. Build. Eng.* 30, 101272. doi:10.1016/j.jobe.2020.101272

Khan, M. I., Fares, G., Abbas, Y. M., and Alqahtani, F. K. (2021). Behavior of non-shear-strengthened UHPC beams under flexural loading: Influence of reinforcement percentage. *Appl. Sci.* 11, 11346. doi:10.3390/app112311346

Khan, M. I., Fares, G., and Abbas, Y. M. (2021). Behavior of non-shear-strengthened UHPC beams under flexural loading: Influence of reinforcement depth. *Appl. Sci.* 11, 11168. doi:10.3390/app112311168

Khan, M. A., Aslam, F., Faisal Javed, M., Alabduljabbar, H., and Deifalla, A. F. (2022). New prediction models for the compressive strength and dry-thermal conductivity of bio-composites using novel machine learning algorithms. *J. Clean. Prod.* 350, 131364. ISSN 0959-6526. doi:10.1016/j.jclepro.2022.131364

Koniki, S., and Prasad, D. R. (2019). Influence of hybrid fibres on strength and stress-strain behaviour of concrete under uni-axial stresses. *Constr. Build. Mat.* 207, 238–248. doi:10.1016/j.conbuildmat.2019.02.113

Kumar, M. V., Niveditha, K., Anusha, B., and Sudhakar, B. (2017). Comparison study of basalt fiber and steel fiber as additives to concrete. *Int. J. Res. Appl. Sci. Eng. Technol.* 5, 2321–9653. www.ijraset.com6 (Accessed November 8, 2019).

Li, B., Chi, Y., Xu, L., Shi, Y., and Li, C. (2018). Experimental investigation on the flexural behavior of steel-polypropylene hybrid fiber reinforced concrete. *Constr. Build. Mat.* 191, 80–94. doi:10.1016/j.conbuildmat.2018.09.202

Li, C., Zhao, M., Geng, H., Fu, H., Zhang, X., and Li, X. (2021). Shear testing of steel fiber reinforced expanded-shale lightweight concrete beams with varying of shear-span to depth ratio and stirrups. *Case Stud. Constr. Mater.* 14, e00550. ISSN 2214 -5095. doi:10.1016/j.cscm.2021.e00550

Li, Y., Zhang, Q., KamiÑski, P., Deifalla, A., Sufian, M., Dyczko, A., et al. (2022). Compressive strength of steel fiber-reinforced concrete employing supervised machine learning techniques. *Materials* 15 (12), 4209. doi:10.3390/ma15124209

Lim, W. Y., and Hong, S. G. (2017). Shear tests for ultra-high performance fiber reinforced concrete (UHPFRC) beams with shear reinforcement. *Int. J. Concr. Struct. Material* 10 (2), 177–188. doi:10.1007/s40069-016-0145-8

Mohammed, H., Ahmed, H., Kurda, R., Alyousef, R., and Deifalla, A. F. (2022). Heat-induced spalling of concrete: A review of the influencing factors and their importance to the phenomenon. *Materials* 15, 1693. doi:10.3390/ma15051693

Naqi, A., and Jang, J. G. (2019). Recent progress in green cement technology utilizing low carbon emission fuels and raw materials: Review. *Sustainability* 11 (537), 1–18.

Navas, F. O., Navarro-Gregori, J., Herdocia, G. L., Serna, P., and Cuenca, E. (2018). An experimental study on the shear behaviour of reinforced concrete beams with macro-synthetic fibres. *Constr. Build. Mater* 169, 888–899. doi:10.1016/j.conbuildmat.2018.02.023

Ortiz Navas, F., Navarro-Gregori, J., Leiva Herdocia, G., Serna, P., and Cuenca, E. (2018). An experimental study on the shear behaviour of reinforced concrete beams with macro-synthetic fibres. *Constr. Build. Mater.* 169, 888–899. ISSN 0950-0618. doi:10.1016/j.conbuildmat.2018.02.023

Pakravan, H. R., Latifi, M., and Jamshidi, M. (2016). Ductility improvement of cementitious composites reinforced with polyvinyl alcohol-polypropylene hybrid fibers. *J. Ind. Text.* 45 (5), 637–651. doi:10.1177/1528083714534712

Shaaban, I., Said, M., Khan, S., Eissa, M., and Elrashidy, Kh. (2021). Experimental and theoretical behaviour of reinforced concrete beams containing hybrid fibres. *Structures* 32, 2143–2160. ISSN 2352-0124. doi:10.1016/j.istruc.2021.04.021

Shen, Z., Deifalla, A. F., Kamiński, P., and Dyczko, A. (2022). Compressive strength evaluation of ultra-high-strength concrete by machine learning. *Materials* 15, 3523. doi:10.3390/ma15103523

Shi, F., Pham, T. M., Hao, H., and Hao, Y. (2020). Post-cracking behaviour of basalt and macro polypropylene hybrid fibre reinforced concrete with different compressive strengths. *Constr. Build. Mater* 262, 120108. doi:10.1016/j.conbuildmat.2020.120108

Sivakumar, V., Karthik, K., Jachin, S. B., and Xavier, C. A. (2020). Experimental investigation on strength properties of hybrid fibre reinforced high strength concrete. *Mat. Today Proc.* doi:10.1016/j.matpr.2020.12.897

Smarzewski, P. (2018). Flexural toughness of high-performance concrete with basalt and polypropylene short fibres. *Adv. Civ. Eng.* 2018, 1–8. doi:10.1155/2018/5024353

Tahenni, T., Bouziadi, F., Boulekbache, B., and Amziane, S. (2021). Experimental and nonlinear finite element analysis of shear behaviour of reinforced concrete beams. *Structures* 29, 1582–1596. ISSN 2352-0124. doi:10.1016/j.istruc.2020.12.043

Tahenni, T., Chemrouk, M., and Lecompte, T. (2016). Effect of steel fibers on the shear behavior of high strength concrete beams. *Constr. Build. Mater.* 105, 14–28. ISSN 0950-0618. doi:10.1016/j.conbuildmat.2015.12.010

Tawfik, M., El-said, A., Deifalla, A., and Awad, A. (2022). Mechanical properties of hybrid steel-polypropylene fiber reinforced high strength concrete exposed to various temperatures. *Fibers* 10, 53. doi:10.3390/fib10060053

Torres, J. A., and Lantsoght, E. O. L. (2019). Influence of fiber content on shear capacity of steel fiber-reinforced concrete beams. *Fibers* 7, 102. doi:10.3390/fib7120102

Tran, T. T., Pham, T. M., and Hao, H. (2020). Effect of hybrid fibers on shear behaviour of geopolymer concrete beams reinforced by basalt fiber reinforced polymer (BFRP) bars without stirrups. *Compos Struct.* 243, 112236. doi:10.1016/j.compstruct.2020.112236

Wang, D., Ju, Y., Shen, H., and Xu, L. (2019). Mechanical properties of high performance concrete reinforced with basalt fiber and polypropylene fiber. *Constr. Build. Mater* 197, 464–473. doi:10.1016/j.conbuildmat.2018.11.181

Xu, L. H., Wu, F. H., Chi, Y., Cheng, P., Zeng, Y. Q., and Chen, Q. (2019). Effects of coarse aggregate and steel fibre contents on mechanical properties of high-performance concrete. *Constr. Build. Mat.* 206, 97–110. doi:10.1016/j.conbuildmat.2019.01.190

Yan, P., Chen, B., Afgan, S., Haque, M. A., Wu, M., and Han, J. (2021). Experimental research on ductility enhancement of ultra-high performance concrete incorporation with basalt fibre, polypropylene fibre and glass fibre. *Constr. Build. Mater* 279, 122489. doi:10.1016/j.conbuildmat.2021.122489

Yang, X., Liang, N., Hu, Y., and Feng, R. (2021). An experimental study of shear resistance for multisize polypropylene fiber concrete beams. *Int. J. Concr. Struct. Mater.* 15, 52–11. doi:10.1186/s40069-021-00492-7

Yavaş, A., Hasgul, U., Turker, K., and Birol, T. (2019). Effective fiber type investigation on the shear behavior of ultrahigh-performance fiber-reinforced concrete beams. *Adv. Struct. Eng.* 22 (7), 1591–1605. doi:10.1177/1369433218820788

Zhang, L. H., Liu, J. Z., Liu, J. P., Zhang, Q. Q., and Han, F. Y. (2018). Effect of steel fiber on flexural toughness and fracture mechanics behavior of ultra-high-performance concrete with coarse aggregate. *J. Mat. Civ. Eng.* 30, 4018323. doi:10.1061/(asce)mt.1943-5533.0002519

Zhang, Y., Wu, B., Wang, J., Liu, M., and Zhang, X. (2019). Reactive powder concrete mix ratio and steel fiber content optimization under different curing conditions. *Materials* 12, 3615. doi:10.3390/ma12213615

Zhong, C., Liu, M., Zhang, Y., Wang, J., Liang, D., and Chang, L. (2020). Study on mechanical properties of hybrid polypropylene-steel fiber RPC and computational method of fiber content. *Materials* 13, 2243. doi:10.3390/ma13102243

Zhou, L., and Wan, S. (2022). Shear behavior of UHPC beams with small shear span to depth ratios based on MSTM. *Case Stud. Constr. Mater.* 16 (2022), e01134. ISSN 2214-5095. doi:10.1016/j.cscm.2022.e01134

Zou, Y., Yu, K., Heng, J. L., Zhang, Z. Y., Peng, H. B., Wu, C. L., et al. (2023a). Feasibility study of new GFRP grid web - concrete composite beam. *Compos. Struct.* 305, 116527. doi:10.1016/j.compstruct.2022.116527

Zou, Y., Zheng, K., Zhou, Z., Zhang, Z., Guo, J., and Jiang, J. (2023b). Experimental study on flexural behavior of hollow steel-UHPC composite bridge deck. *Eng. Struct.* 274, 115087. doi:10.1016/j.engstruct.2022.115087